Optimisation of the synthesis of ZrC coatings in a radio frequency induction-heating chemical vapour deposition system using response surface methodology

S Biira[1,2*], PL Crouse[3], H Bissett[4,] BAB Alawad[1], TT Hlatshwayo[1], JT Nel[4], JB Malherbe[1]

[1] *Department of Physics, University of Pretoria, Pretoria, 0002 South Africa*

[2]*Department of Physics, Busitema University, PO Box 236, Tororo, Uganda*

[3]*Department of Chemical Engineering, University of Pretoria, 0002 South Africa*

[4]*Applied Chemistry Division, The South African Nuclear Energy Corporation (Necsa), P.O Box 582, Pretoria, 0001 South Africa*

**Corresponding Author: Tel.: +27611 894 594, E-mail address: bsaphina@yahoo.co.uk*

Abstract

A chemical vapour deposition process using radio frequency induction heating operating at atmospheric pressure was developed for the deposition of ZrC coatings. The precursors utilised in this process were zirconium tetrachloride and methane as zirconium and carbon sources respectively, in an excess of hydrogen. Additionally, a stream of argon was used to, first, remove oxygen from the reactor and then to sweep the vapourised $ZrCl_4$ at 300 °C to the reaction chamber. The ZrC coatings were deposited on graphite substrates at substrate temperatures in the range of 1200 °C –1600 °C. The molar ratio of $CH_4/ZrCl_4$ was varied from 6.04 to 24.44. Before the start of the deposition process, thermodynamic feasibility analysis for the growth of ZrC at atmospheric pressure was also carried out. Response surface methodology was applied to optimise the process parameters for the deposition of ZrC coatings. A central composite design was used to investigate the effects of temperature and molar ratio of $CH_4/ZrCl_4$ on the growth rate, atomic ratio of C/Zr and crystallite size of ZrC

coatings. Quadratic statistical models for growth rate and crystallite size were established. The atomic ratio of C/Zr followed a linear trend. It was found that an increase in substrate temperature and $CH_4/ZrCl_4$ ratio resulted in increased growth rate of ZrC coatings. The carbon content (and concomitantly the atomic ratio of C/Zr) in the deposited coatings increased with temperature and molar ratio of $CH_4/ZrCl_4$. The substrate temperature of 1353.3°C and the $CH_4/ZrCl_4$ molar ratio of 10.41 was determined as the optimal condition for growing near-stoichiometry ZrC coatings. The values were 1.03, 6.05 μm/h and 29.8 nm for C/Zr atomic percentage ratio, growth rate and average crystallite size respectively.

Keywords: Zirconium carbide, chemical vapour deposition, radiofrequency induction heating, response surface design, growth rate, crystallite size, C/Zr ratio.

1 Introduction

Generation IV high temperature nuclear reactors use TRISO (tristructural isotropic) particles for containment of radioactive fission products [1]. TRISO particles consist of uranium oxide coated uniformly with low density pyrocarbon, high density inner pyrocarbon, silicon carbide (SiC), and dense outer pyrocarbon [2]. In these particles SiC is the main barrier for containing solid fission products. These particles retain most fission products with the exception of silver at temperatures below 1000 °C. In a recent review paper by Malherbe on SiC [3], the problems of the diffusion of silver and other fission products in SiC was extensively discussed. In the same review, it was suggested that it would be advantageous to add a thin ZrC layer (in addition to the normal SiC layer) to the TRISO layer system because it is a better barrier than SiC against Ag diffusion and is more resistant against palladium attack [4,5].

ZrC has a high melting temperature of 3540 °C, and relatively low vapour pressure compared to SiC, which begins to decompose at 1500 °C [6]. ZrC also has a low neutron capture cross

section, good thermal shock resistance, relatively low density, excellent thermal stability, and high hardness [7,8]. It is important to note that the properties of ZrC coatings depend on a number of factors such as chemical composition, crystallite size and morphology, orientations of crystal planes, structural defects, porosity, and the presence of impurities. These factors are a function of the methods and conditions used in growing ZrC coatings. Chemical vapour deposition (CVD) produces coatings with very low levels of impurities and low porosity [9], which is why it is the preferred method.

Compared to SiC, little research has been published on the use of ZrC in nuclear reactors. The main reason is probably that SiC has proven nuclear applications, and other desirable physical properties (e.g. a wide bandgap semiconductor, it's the second hardest natural material, etc.). Another reason for this might be that it is difficult to grow good quality ZrC.

In this study, the aim is to introduce a statistical optimisation method to grow ZrC coatings in a CVD system using a response surface methodology. This method allows one to determine the deposition parameters for obtaining specific coating properties, e.g. ZrC coatings with a specific composition. This has not yet been reported for ZrC film growth. The paper also details the development of a deposition process for the preparation and optimisation of ZrC coatings from $ZrCl_4$-Ar-CH_4-H_2 precursors using induction thermal CVD at atmospheric pressure. The objectives were: (1) to fabricate and develop the CVD system; and (2) to investigate the microstructure and composition of ZrC coatings deposited as a function of the input variables. In this study ZrC coatings were produced by CVD at temperatures ranging from 1200 °C to 1600 °C and $CH_4/ZrCl_4$ molar ratios from 6.04 to 24.44. After choosing temperature and the $CH_4/ZrCl_4$ ratio as the most important variables influencing the properties of ZrC, in order to achieve optimum conditions for growing ZrC coatings, a statistical experimental design methodology (central composite design) was applied to explore the effects of these variables [10]. Other deposition conditions such as total reactor

pressure, deposition time, reactor geometry, hydrogen flow and carrier gas and its flow have been maintained constant throughout this experimental process.

2 Experimental

2.1 Apparatus

In this study a vertical-wall thermal CVD system, as indicated in Figure 1, was developed in-house at Necsa (The South African Nuclear Energy Corporation). The system consists of the following basic components: (1) a 10 kW radio frequency (RF) power supply system; (2) a gas supply and delivery system (including a zirconium tetrachloride vapouriser); (3) the reactor system (including a cylindrical graphite reaction tube, heated by an induction coil, in which the substrate is mounted on a stage); and (4) an exhaust/scrubber system ($CaCO_3$) for extracting and neutralising HCl gas which formed as a by-product during the decomposition reaction and unreacted $ZrCl_4$ gas.

The gap between the four-turn helical copper coils and the graphite reaction chamber was kept minimal to ensure good RF coupling with the coil. This distance was sufficient to accommodate the thermal insulation (ceramic material) to reduce heat transfer from the heated graphite reaction chamber to the coil. The ceramic material also secured the graphite reaction chamber at the centre of the coil in a fixed position

The high density graphite tube had an inner diameter of 2.5 cm and a length of 30 cm. An inlet and outlet at the top and bottom of the graphite tube permitted the flow of the gases past the heated substrates mounted on substrate stage. The substrate temperature was measured by an infra-red optical pyrometer through a quartz viewing window at the top of the flange. Argon, methane, and hydrogen flow were controlled using pre-calibrated rotameters. To avoid $ZrCl_4$ from clogging the gas feed lines, all gas feed lines were heated to 300 °C by an

electric heat tracing tape. Figure 1(a) and (b) show the reactor set-up and, the process and instrumentation diagram of the CVD system respectively.

The $ZrCl_4$ vaporisation system consisted of an oven and a stainless steel tube fitted with inlet and outlet feed lines. $ZrCl_4$ powder was placed in a graphite boat before it was placed inside the stainless steel tube. $ZrCl_4$ powder is very hygroscopic. Precautions were taken to avoid exposure of the $ZrCl_4$ powder to atmospheric moisture as far as possible. The inlet and outlet feed lines allowed argon to sweep through freely. To determine and optimise the vapour pressure of $ZrCl_4$ for the deposition of ZrC coatings, $ZrCl_4$ was heated in vacuum and under argon for 3 minutes for each temperature. Figure 2 shows a plot of the pressure as a function of temperature, measured under vacuum and at argon pressure of 11 kPa. For $ZrCl_4$ under argon, the total pressure measured was the sum of the pressure of the $ZrCl_4$ vapour and the argon partial pressure. The presence of argon did not change the pressure-temperature trend. Basing on this calibration curve, a working temperature of 300 °C was selected.

The vaporised $ZrCl_4$ was delivered into the reaction chamber by an argon flow, subsequently mixed with the methane and the hydrogen feed. The mass flow rate of $ZrCl_4$ was controlled by varying the argon flow rate. The $ZrCl_4$ mass transfer rate as a function of argon flow rate is shown in Figure 3. The calibration curve was obtained by flowing argon through the $ZrCl_4$ powder at different argon flow rates each for 20 minutes, and determining the mass difference every after each run.

2.2 Raw materials and deposition process of ZrC coatings

The substrates of diameter 11 mm and thickness 3 mm were cut from bulk high density (1.71g cm^{-3}) graphite discs. These graphite substrates were hand polished on a polishing wheel using 1000 grit silicon carbide paper. They were then sequentially cleaned by ultrasonic agitation with acetone, ethanol and then demineralised water for 20 minutes each.

The clean substrates were dried in an oven at 200 °C for 2 hours. Before deposition, the substrates were mounted on the clean graphite substrate stage inside the graphite reaction chamber. The reactor was then flushed by continuously pressurising and depressurising it using argon in order to remove air (oxygen) and atmospheric moisture.

The precursors used in deposition of ZrC were zirconium tetrachloride ($ZrCl_4$, 99.5% pure manufactured by Sigma-Aldrich (Pty) Ltd) and methane (CH_4, 99.99% pure) as zirconium and carbon sources respectively. $ZrCl_4$ was carried from the vaporisation chamber to the reaction chamber by argon (Ar, 99.999% pure). Hydrogen gas (H_2, 99.999% pure) was used to provide reducing and diluting environment for $ZrCl_4$ vapour. Methane, hydrogen and argon flow rates were measured by previously calibrated flow meters and directed into the reaction chamber as shown in Figure 1(b). The deposition was carried out at atmospheric pressure (which was 87 kPa absolute at location) for 2 hours, excluding a 10 minute period for allowing the substrates to reach thermal equilibrium.

2.3 Design of experiments and response surface methodology

The ZrC deposition process was investigated using a central composite design (CCD). Two independent variables (substrate temperature, $X_1=T$) and molar ratio $CH_4/ZrCl_4$ ($X_2=M$) were chosen. The experimental design was studied using DESIGN-EXPERT® 7.0 [11], a statistical software package. Substrate temperature and molar ratio $CH_4/ZrCl_4$ were all studied, each at five levels coded as $-\alpha$, -1, 0, 1 and α. Figure 4 shows the CCD for the two variables. Thirteen experimental points were generated. These included four axial points, four factorial points, and five replicated centre points, as shown in Table 1. Coding of levels allows the analysis of input variables having orders of magnitude (or range) difference between them, i.e. this prevents the ones with large values to dominate the lower value ones in the statistical analysis. It involves transforming the actual values of each input variable into dimensionless

coordinates (values). Equation 1 was applied to transform actual values (X_i) into a coded values (x_i) based on the experimental design [12,13]:

$$x_i = \left(\frac{X_i - X_i^{o}}{\Delta X_i} \right) \alpha \quad (1)$$

If in the actual scale the upper value is X_h and the lower value is X_l, then the centre point $X_i^0 = (X_h + X_l)/2$ and distance between the upper or lower and centre point $\Delta X_i = (X_h - X_l)/2$. α is the major coded limit value of the experimental matrix. For two input variables $\alpha = \sqrt{2} = 1.41421$ [12].

Growth rate (Y_1), atomic ratio of C/Zr (Y_2) and crystallite size (Y_3) were selected as dependent variables (responses). For the purpose of analysing the raw data and testing the goodness of fit of the model, an analysis of variance (ANOVA) was implemented. The testing of model adequacy involved test for significance of the regression model, test for significance on model coefficients and test for lack of fit [14]. The statistical tests *p*-value, *F*-value, *R*-squared, predicted *R*-squared, and adjusted *R*-squared were used as quality indicators. The model with the *p*-value (Probability > *F*) less than 0.05 is considered to be statistically significant [10]. *R*-squared known as the coefficient of determination is a measure of variability in the observed response values that can be explained by the experimental independent variables and their interactions. The *R*-squared value range between 0 and 1 (0% and 100%). The model is regarded very strong and with better predication of the response when *R*-squared is close or equal to 1 [15]. The adjusted *R*-squared corrects the *R*-squared value for the sample size and for the number of terms in the model. The closer their values to one another, the better the model is [16]. Another component in assessing the model suitability is the concept “adequate precision” , which compares the range of predicted values at design points to avarage design error, and measures the signal–to–noise ratio. A value of greater than 4 is acceptable [16].

2.4 Characterisation of ZrC coatings

X-ray diffraction (XRD) analysis was used to determine the crystal structure and phase composition of the deposited ZrC coatings. This was carried out using a Bruker XRD D8 Advance with a Cu K_α radiation source (λ=1.54056 Å) within the recording range of 15^o to 125^o and a step size of 0.04. The working potential and the corresponding current used during spectrum acquisition were 1 kV and 40 mA respectively. The average crystal sizes were calculated using the Scherrer formula.

The surface morphology of the as deposited ZrC coatings was analysed using an ultrahigh resolution field-emission scanning electron microscopy (FE-SEM, Zeiss Ultra Plus) with operating voltage set at 1 kV. The elemental composition of the coatings was characterised by energy-dispersive spectroscopy (EDS, Oxford Instruments) mounted on a FE-SEM Zeiss Ultra Plus. The operating voltage while collecting the EDS spectra was set at 20 kV. To cater for in homogeneity in the sample, five measurements from five different regions on the surface of each sample were taken and the average of this was taken as the 'true' elemental composition of the sample. The effect of substrate temperature and molar ratio $CH_4/ZrCl_4$ on C-Zr content in the deposited coatings was studied. The mass of the substrate before and after deposition was measured by an electronic mass balance with a precision of 0.0001 g.

3 Results and Discussions

3.1 Thermodynamics

The overall reaction, considering only reagents and the two main products, is:

$$ZrCl_4(g) + CH_4(g) = ZrC(s) + 4HCl(g) \quad (2)$$

The Gibbs free energy change for the reaction as a function of temperature, and the corresponding equilibrium constant [17], are shown in Figure 5. The temperature-dependent values of Gibbs free energy of formation of methane, zirconium carbide, hydrogen chloride

gas and zirconium tetrachloride at atmospheric pressure were obtained from JANAF thermodynamic tables [18,19]. The Gibbs free energy change becomes zero at 1600.8 K (1327.6 °C).

A more sophisticated thermodynamic approach, taking into account all possible product species, is via the minimisation of the system Gibbs free energy [20]. Figure 6 shows speciation results obtained using this method. The software HSC Chemistry [21] was used for this purpose. It is clear from Figure 6 that the growth of ZrC is possible at temperatures as low as 900 °C, but higher yields are expected as the temperature is increased. The temperature range predicted from the plots in Figure 5 and Figure 6 is similar to those reported in the literature [22–24].

It should be noted that methane is unstable at temperatures higher than 400 °C, yielding carbon and hydrogen upon decomposition. On the other hand, hydrogen does not reduce $ZrCl_4$, in the absence of other substances, with in this experimental range. The formation of ZrC is thus controlled by the presence of methane, with its decomposition making carbon available for the reaction process. Independent deposition of carbon alone is thus possible. The reaction rate of methane with zirconium tetrachloride is strongly influenced by the temperature of the substrate surface. As the temperature increases the chemical reaction is pushed to the region of high yields of ZrC and concomitantly higher degrees of dissociation of $ZrCl_4$.

3.2 Growth rate of Zirconium carbide

The growth rate Y_1 (change in coating thickness per unit time) was estimated using the mass increase of the substrate. The coating thickness was obtained using Equation (3):

$$Y_1 = \frac{M}{tS\rho_{ZrC}} \tag{3}$$

where M is the mass of the coatings, S is the surface area of the substrate, ρ_{ZrC} is the density of zirconium carbide (6.59 kg m^{-3}) and t is the deposition time. The raw experimental data are presented in Table 2.

The use of a constant zirconium carbide density value obviously introduces an error into the calculation of the growth rate. From the analysis of the effect of temperature and $CH_4/ZrCl_4$ on the growth rate by RSM, the best fitted-model was found to be quadratic. The relationship between the growth rate (response Y_1) and the independent variables (temperature and $CH_4/ZrCl_4$) was represented in actual and coded factors by the regression Equations (4a) and (4b) respectively. Table 3 presents the ANOVA results for the growth rate of ZrC coatings. This model was also statistically significant with a *p*-value less than 0.05 (95% confidence). As required the lack-of-fit was non-significant with an *F*-value and *p*-value of 4.28 and 0.0969 respectively. The coefficient of determination *R*-squared and adjusted *R*-squared values were 96% and 93%, indicating that the regression model give a good description of the relationship between the temperature and $CH_4/ZrCl_4$ (independent variables), and the growth rate (response). Therefore this model can be used to navigate the design space reliably.

$$Y_1 = -87.22 + 0.13T - 0.75M + 8.7\times10^{-4}TM - 4.81\times10^{-5}T^2 - 8.57\times10^{-3}M^2 \quad (4a)$$

$$Y_1 = 7.60 + 1.41A + 1.31B + 0.80AB - 0.96A^2 - 0.36B^2 \quad (4b)$$

Figure 7 shows the response surface contour plot illustrating the effects of substrate temperature and $CH_4/ZrCl_4$ molar ratio on the growth rate. The dots represent the experimental values (given in Table 2). The numbers in rectagles denote the value of the response along the given contour given by Equation 4. The numerical symbol "5" represents the five replicated centre points. Generally, increasing temperature and $CH_4/ZrCl_4$ ratio increase the coating growth rate. The effect of temperature on the ZrC growth rate is expected both thermodynamically, and from a kinetic viewpoint. A high $CH_4/ZrCl_4$ molar ratio

increases the availability of carbon in the reaction zone, which arguably will increase both the nucleation and growth rate.

3.3 Crystallographic structure and phase composition

Figure 8 shows typical XRD patterns of ZrC coatings deposited at substrate temperature of 1259 ºC and 1541 ºC for $CH_4/ZrCl_4$ of 8.73 and 21.7. Ten reflections (111), (200), (220), (311), (222), (400), (331), (420), (422) and (511) of ZrC coatings were observed These reflections indicate that polycrystalline face-centred cubic structure of the ZrC coating has been deposited when matched with the International Centre for Diffraction Data (ICDD) file number 03.065-8833. As the substrate temperature and the $CH_4/ZrCl_4$ molar ratio were increased, carbon peak started to emerge whose intensity increased with increasing temperature and $CH_4/ZrCl_4$ ratio. EDS analysis show that the atomic percentage ratio of C/Zr varied from 1.03 to 2.57 as the temperature increased from 1200 ºC to 1600 ºC at various $CH_4/ZrCl_4$ ratios as indicated in Table 2. It was observed that at low substrate temperature the increase in $CH_4/ZrCl_4$ molar ratio did not cause a significant change in C/Zr as compared to higher substrate temperatures (see Figure 8 and Table 2).

Table 4 gives the ANOVA results for a linear regression model for the atomic ratio of C/Zr. This relationship between the independent variables and the response in terms of actual and coded factors is illustrated by the linear regression Equation (5a) and (5b) respectively. The model is significant with a *p*-value of less than 0.05 and an F-value of 6.58. The lack-of-fit of the model terms is non-significant as required. The *R*-squared and adjusted *R*-squared values are 56.83% and 48.20% respectively. The *R*-squared and adjusted *R*-squared values obtained are close to each other, though far from 100%. Since the overall model is significant and lack of fit is non-significant, the R-squared value may not affect the interpretation of the

relationship between the independent variables (temperature and $CH_4/ZrCl_4$) and the response (C/Zr).

$$Y_2 = -1.63 + 1.55 \times 10^{-3} T + 0.054M \quad (5a)$$

$$Y_2 = 1.36 + 0.22A + 0.35B \quad (5b)$$

The contour plot in Figure 9 further illustrates the relationship of temperature and $CH_4/ZrCl_4$, and atomic ratio of C/Zr. The same kind of information/notation as with Figure 9 was used *mutatis mutandis* in Figure 10. There was an increase in C/Zr atomic percentage ratio as both substrate temperature and $CH_4/ZrCl_4$ molar ratio increased. The increase in carbon content may be attributed to partly by the differences in the decomposition rates of methane and $ZrCl_4$ at higher temperatures in the reaction zone. As it can be seen from Figure 6 methane decomposes into carbon as earlier as at 420 °C. Zr-containing species remains in gaseous form throughout the experimental range. This may result into excess carbon. The deposition of free carbon leads to an increased C/Zr ratio in the deposited coatings and carbon inclusions at the high ratios. The presence of free carbon in ZrC coatings at elevated deposition temperatures was also reported by Wang et al. [24]. An increase in the $CH_4/ZrCl_4$ ratio provides more carbon in the reaction zone which also leads to increased carbon content in the ZrC coatings. Studies have indicated that the properties of ZrC vary with its stoichiometry (C/Zr atomic percentage ratio) [9]. For example Yang et al. [25] indicated that the C/Zr ratio had a notable effect on the irradiation response of zone-refined ultra-high pure ZrC. They noted that the sub-stoichiometric ZrC samples (C/Zr<1) had an improved irradiation resistant microstructure compered to hyper-stoichiometric ZrC samples (C/Zr>1). Huang et al. [26] reported that ZrCx material after a proton irradiation at 800 °C was highly decorated with dislocation loops. The loop size and density depended both on dose and stoichiometry with $ZrC_{1.2}$ showing quite different behaviour compared to the lower C-ratio stoichiometries.

Information about the oxidation behaviour for various ZrC stoichiometries is limited. However in the review by Katoh et al.[9], they speculated that the excess carbon in ZrC can

change the oxidation behaviour of ZrC materials. The excess carbon can increase the production of CO_2 which may increase the chances of inter-crystalline fracture and below normal temperature fracture.

Crystallite size

The average crystallite size, Y_3 was calculated from Scherrer formula given by Equation (6):

$$Y_3 = \frac{0.94\lambda}{\Gamma \cos\theta} \tag{6}$$

where λ is the wave length of the characteristic X-ray, Γ is the full width at half maxima and θ is the Bragg diffraction angle.

The crystallite size in polycrystalline materials significantly affects the mechanical properties of the material [27,28]. The average crystallite size varied from 21.8 nm to 34.1 nm as the temperature increased from 1200 °C to 1600 °C at various $CH_4/ZrCl_4$ ratios as indicated in Table 2. The execution of RSM produced the regression Equations (7a) and (7b) that represents the relationship between the crystallite size and the independent variables in actual and coded factors respectively. Table 5 gives the ANOVA results for the average crystallite size.

$$Y_3 = -129.69 + 0.17T + 4.28M - 1.06\times10^{-3}TM - 4.81\times10^{-5}T^2 - 8.57\times10^{-3}M^2 \tag{7a}$$

$$Y_3 = 32.82 + 1.72A - 0.21B - 0.97AB - A^2 - 4.67B^2 \tag{7b}$$

A quadratic model was found to be statistically significant. The model's corresponding *p*-value is less than 0.05 (95% confidence). The lack-of-fit is not significant as can be seen from the *F*-value and *p*-value of 4.93 and 0.0787 respectively. The *R*-squared and adjusted *R*-squared values are 91% and 85%, indicating that the regression model gives a good description of the relationship between the temperature and $CH_4/ZrCl_4$ (independent variables), and the crystallite size (response).

To fully describe the interactions and the quadratic effect of the temperature and $CH_4/ZrCl_4$ on crystallite size, the response surface analyses was plotted in the contour graph given in Figure 10. Again, the same kind of information/notation as with Figure 9 was used *mutatis mutandis* in Figure 10. It can be observed that the average crystallite size increases as temperature and $CH_4/ZrCl_4$ ratios increase. This is because increasing temperature increases atomic mobility which favour crystal growth. There should also be a sufficient $CH_4/ZrCl_4$ concentration to facilitate the reaction mechanism. It can also be observed from Figure 10 that as the temperature and $CH_4/ZrCl_4$ increase further the crystallite size decreases. The reason for this may be due to increased amount of free carbon which acts as an impurity during ZrC crystal growth. This co-deposition of free carbon may retard the growth of ZrC crystallites.

3.4 Surface morphology

The variation of the surface morphology of the ZrC coatings deposited at varying substrate temperatures and $CH_4/ZrCl_4$ molar ratios is highlighted in Figure 11. The SEM images of the ZrC coatings shown in Figure 11 were prepared at 1259 °C and 1541 °C for $CH_4/ZrCl_4$ molar ratios of 8.73 and 21.75. For the coatings prepared at 1259 °C $CH_4/ZrCl_4$ of 8.73, the surface morphology shows small grains rounded by lots of cavities. When the $CH_4/ZrCl_4$ was increased to 21.75 the size of the grain size increased and the amount and size of cavities reduced. The grain also tend to cluster to gather forming cauliflower-like structure. This might be an indication of small grains agglomerating to form much bigger grains during deposition. Increasing the $CH_4/ZrCl_4$ molar ratio increases the amount of carbon-containing species that would readily combine with Zr-containing species to form ZrC. So coating growth was increasingly not limited by carbon availability. These grains became much denser and bigger as the deposition temperature increased to 1541 °C for $CH_4/ZrCl_4$ at 8.73. There was increased particles agglomeration and islands became visible. No cavities were visible

between the particles. This may be attributed to the increase in the mobility of the deposited molecules on the substrate surfaces as the temperature was increased which might have resulted in increased lateral diffusion and clustering of the atoms at the surface of the substrate. Keeping the temperature at 1541 °C and increasing the $CH_4/ZrCl_4$ molar ratio to 21.75, the surface of the coatings became much smooth with almost no islands. This observation may be explained in reference to Section 3.3. Increase in temperature and $CH_4/ZrCl_4$ ratio increased growth rate and the carbon impurities in the coatings. The carbon impurities may act as additional nucleation sites which will increase the growth on the size of particle observed and levelling of the islands. From these results, it is quite clear that both substrate temperature and $CH_4/ZrCl_4$ molar ratio had a significant impact on the surface morphology of the deposited coatings.

3.5 Optimisation of the experimental and model results

Following the examination of the regression equations and the contour plots representing the independent variables and responses, additional optimisation process was carried out using Design Expert software. Our target was to maximise growth rate and minimise the amount of free carbon in the deposited coatings. These two responses (factors) have a direct influence on other response (crystallite size) generated. It can be observed from Section 3.2, that the value of C/Zr ratio is increased by increasing substrate temperature and $CH_4/ZrCl_4$ molar ratio or both. Therefore these two independent variables must be minimized. The optimal substrate temperature and $CH_4/ZrCl_4$ molar ratio were determined to be 1353.3 °C and 10.41 respectively. At these conditions the predicted growth rate (Y_1), C/Zr atomic percentage ratio (Y_2) and crystallite size (Y_3) were 6.05 µm/h, 1.03 and 29.48 nm respectively. The combined statistical desirability for these optimised values was found to be 0.65. Alternatively, one can solve Equations 4, 5 and 7 to obtain the targeted conditions for the desired responses.

4 Conclusion

ZrC coatings were deposited on graphite substrates at atmospheric pressure CVD using an in-house built RF induction reactor. The experimental and thermodynamic results illustrated the substrate temperatures and $CH_4/ZrCl_4$ ratio as having a major influence on ZrC growth kinetics. The XRD results showed the formation of ZrC material and some amounts of free carbon. The intensity of carbon peaks increased with increasing temperatures and or $CH_4/ZrCl_4$. The average crystallite size, growth rate and stoichiometry (C/Zr ratio) of ZrC coatings were determined as functions of substrate temperature and $CH_4/ZrCl_4$ ratio. The experimental raw results were analysed by the response surface methodology (RSM) to give a correlation between the responses (crystallite size, growth rate and composition) and the chosen important independent variables (substrate temperature and $CH_4/ZrCl_4$ ratio). Mathematical regression representations were obtained and are useful for visualising the theoretical ZrC coatings growth rate, crystallite size and stoichiometry changes. The graphical representation further displays the patterns and trends of their behaviour. The optimum conditions for producing a relative thick near-stoichiometry ZrC coatings (i.e. C/Zr of 1.03 and growth rate of 6.05 μm/h) with crystallite size of 29.8 nm were determined as 1353.3 °C for substrate temperature and 10.14 for $CH_4/ZrCl_4$ molar ratio. The stoichiometric ZrC coatings are promising for their application as fission products barrier in the nuclear fuel TRISO particle. The results from the SEM micrographs indicate that the growth of the particle size increased with both substrate temperature and or $CH_4/ZrCl_4$ molar ratio. The surface of the coatings became more uniform with no noticeable cavities at high temperature and $CH_4/ZrCl_4$ ratios.

Acknowledgements

The authors would like to thank Mr T. Ntsoane from NECSA for his assistance with XRD analysis, University of Pretoria, Busitema University and African Union for financial support. Necsa is highly appreciated for the provision of experimental materials and laboratory space. The authors also would like to thank the Department of Science and Technology of South Africa through the Nuclear Materials Development Network of the Advanced Metals Initiative.

5 References

[1] I.E. Porter, T.W. Knight, M.C. Dulude, E. Roberts, J. Hobbs, Design and fabrication of an advanced TRISO fuel with ZrC coating, Nucl. Eng. Des. 259 (2013) 180–186.

[2] E. López-Honorato, J. Boshoven, P.J. Meadows, D. Manara, P. Guillermier, S. Jühe, et al., Characterisation of the anisotropy of pyrolytic carbon coatings and the graphite matrix in fuel compacts by two modulator generalised ellipsometry and selected area electron diffraction, Carbon N. Y. 50 (2012) 680–688.

[3] J.B. Malherbe, Diffusion of fission products and radiation damage in SiC, J. Phys. D. Appl. Phys. 46 (2013) 473001.

[4] T.M. Besmann, R.E. Stoller, G. Samolyuk, P.C. Schuck, S.I. Golubov, S.P. Rudin, et al., Modeling Deep Burn TRISO particle nuclear fuel, J. Nucl. Mater. 430 (2012) 181–189.

[5] K. Sawa, S. Ueta, Research and development on HTGR fuel in the HTTR project, Nucl. Eng. Des. 233 (2004) 163–172.

[6] N.G. Van Der Berg, J.B. Malherbe, a. J. Botha, E. Friedland, Thermal etching of SiC, Appl. Surf. Sci. 258 (2012) 5561–5566.

[7] H.O. Pierson, Handbook of Refractory Carbides & Nitrides: Properties, Characteristics, Processing and Apps., William Andrew, 1996.

[8] Y.S. Won, V.G. Varanasi, O. Kryliouk, T.J. Anderson, L. McElwee-White, R.J. Perez, Equilibrium analysis of zirconium carbide CVD growth, J. Cryst. Growth. 307 (2007) 302–308.

[9] Y. Katoh, G. Vasudevamurthy, T. Nozawa, L.L. Snead, Properties of zirconium carbide for nuclear fuel applications, J. Nucl. Mater. 441 (2013) 718–742.

[10] D.C. Montgomery, Design and analysis of experiments, John Wiley & Sons, 2008.

[11] Stat-Ease, Design expert version 7.0.0, Stat-Ease Inc. (2005).

[12] M.A. Bezerra, R.E. Santelli, E.P. Oliveira, L.S. Villar, L.A. Escaleira, Response surface methodology (RSM) as a tool for optimization in analytical chemistry, Talanta. 76 (2008) 965–977.

[13] D. Bas, I.H. BoyacI, Modeling and optimization I: Usability of response surface methodology, J. Food Eng. 78 (2007) 836–845.

[14] R.H. Myers, D.C. Montgomery, C.M. Anderson-Cook, Response surface methodology: process and product optimization using designed experiments, John Wiley & Sons, 2016.

[15] R.L. Mason, R.F. Gunst, J.L. Hess, Statistical Design and Analysis of Experiments, 2003.

[16] A. Vohra, T. Satyanarayana, Statistical optimization of the medium components by response surface methodology to enhance phytase production by Pichia anomala, Process Biochem. 37 (2002) 999–1004.

[17] X.-T. Yan, Y. Xu, Chemical vapour deposition: an integrated engineering design for advanced materials, Springer Science & Business Media, 2010.

[18] M.W. Chase Jr, J.L. Curnutt, R.A. McDonald, A.N. Syverud, JANAF thermochemical tables, 1978 supplement, J. Phys. Chem. Ref. Data. 7 (1978) 793–940.

[19] NIST, NIST-JANAF Thermochemical Tables, NIST-JANAF Thermochem. Tables. (2013). http://kinetics.nist.gov/janaf/ (accessed July 30, 2015).

[20] S. Jarungthammachote, A. Dutta, Equilibrium modeling of gasification: Gibbs free energy minimization approach and its application to spouted bed and spout-fluid bed gasifiers, Energy Convers. Manag. 49 (2008) 1345–1356.

[21] Outotec, HSC Chemistry 7 (Thermo-chemical software), (2007).

[22] J. Wagner, C. Mitterer, M. Penoy, C. Michotte, W. Wallgram, M. Kathrein, The effect of deposition temperature on microstructure and properties of thermal CVD TiN coatings, Int. J. Refract. Met. Hard Mater. 26 (2008) 120–126.

[23] Q. Liu, L. Zhang, L. Cheng, Y. Wang, Morphologies and growth mechanisms of zirconium carbide films by chemical vapor deposition, J. Coatings Technol. Res. 6 (2009) 269–273.

[24] Y. Wang, Q. Liu, J. Liu, L. Zhang, L. Cheng, Deposition mechanism for chemical vapor deposition of zirconium carbide coatings, J. Am. Ceram. Soc. 91 (2008) 1249–1252.

[25] Y. Yang, W.-Y. Lo, C. Dickerson, T.R. Allen, Stoichiometry effect on the irradiation response in the microstructure of zirconium carbides, J. Nucl. Mater. 454 (2014) 130–135.

[26] Y. Huang, B.R. Maier, T.R. Allen, Irradiation-induced effects of proton irradiation on zirconium carbides with different stoichiometries, Nucl. Eng. Des. 277 (2014) 55–63.

[27] B.D. Cullity, S.R. Stock, Elements of X-ray Diffraction, Pearson, 2001.

[28] S. Veprek, Recent search for new superhard materials: Go nano!, J. Vac. Sci. Technol. A. 31 (2013) 50822.

Figures and Tables

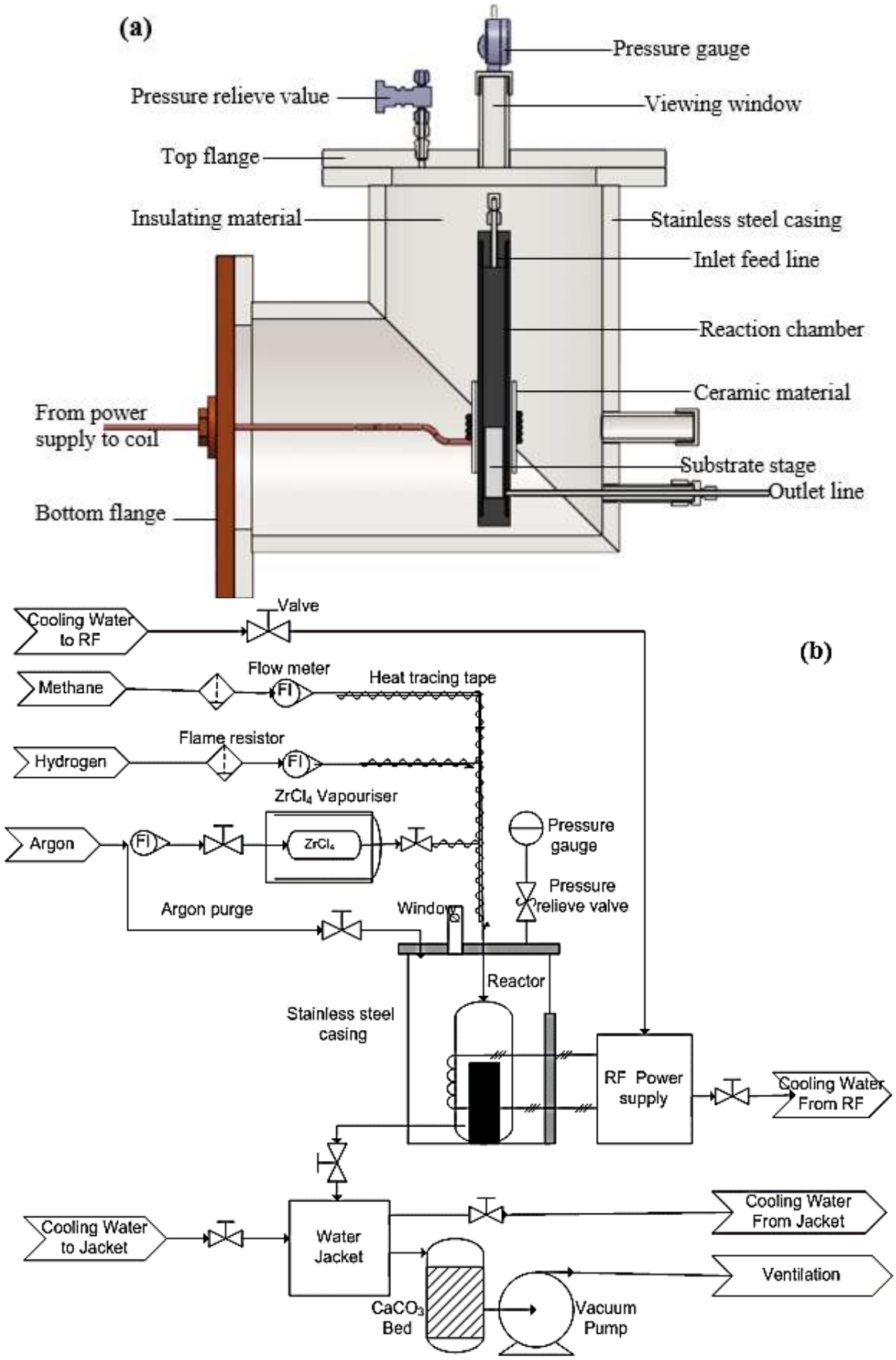

Figure 1**:** *(a) Schematic diagram of the CVD reactor system. (b) Process and instrumentation diagram for the CVD reactor set-up*

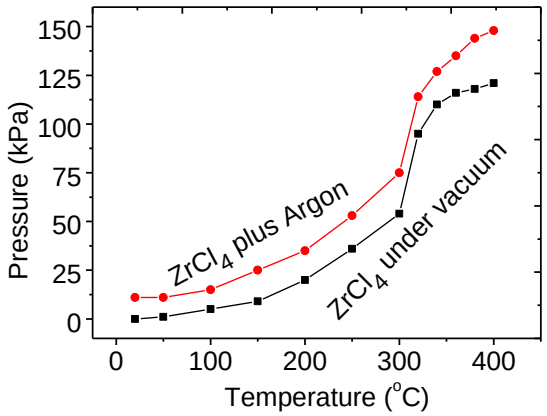

Figure 1**:** *Variation of pressure in the vaporiser with temperature.*

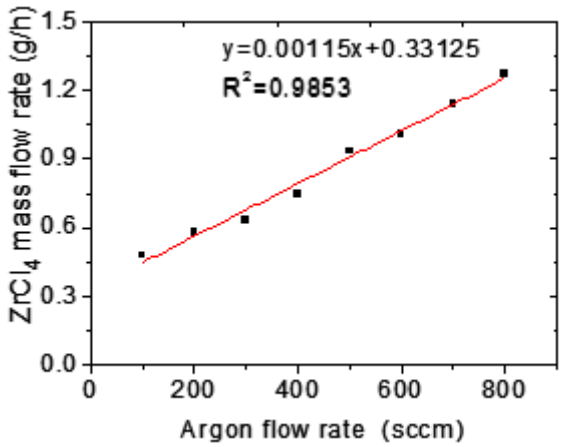

Figure 3: *Calibration curve of $ZrCl_4$ mass flow rate in argon.*

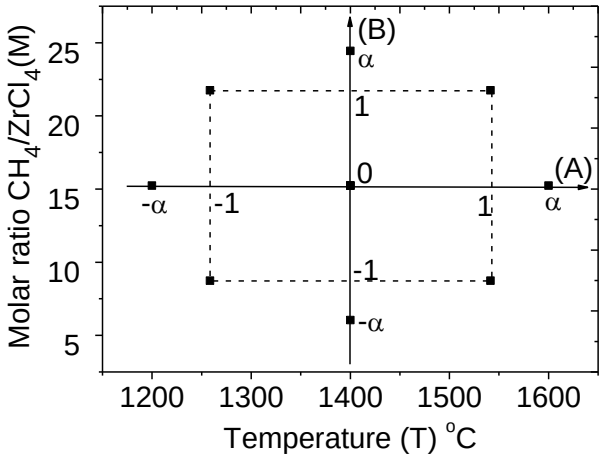

Figure 4*: CCD of temperature and $CH_4/ZrCl_4$ in actual and coded terms.*

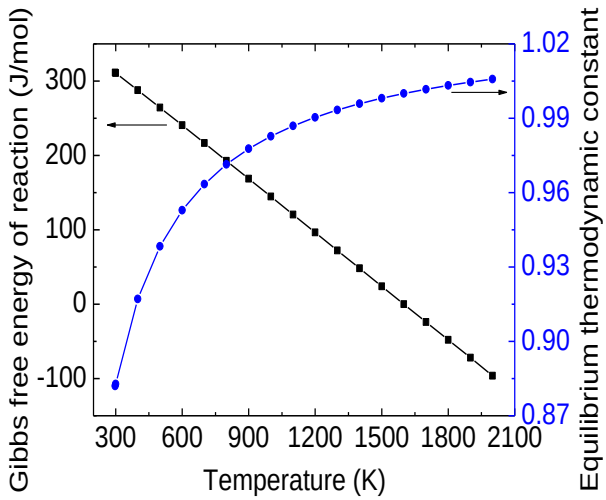

***Figure 5**: Ellingham diagram for stoichiometric ZrC from $ZrCl_4$ and CH_4.*

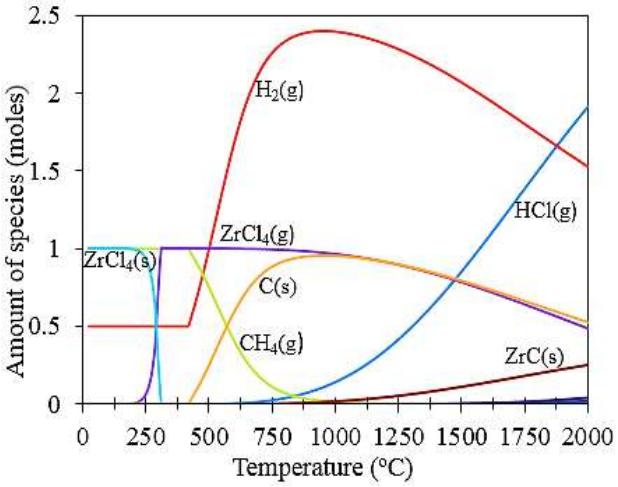

***Figure 6**: Temperature dependent speciation curves of the $ZrCl_4$-CH_4-H_2 feed system.*

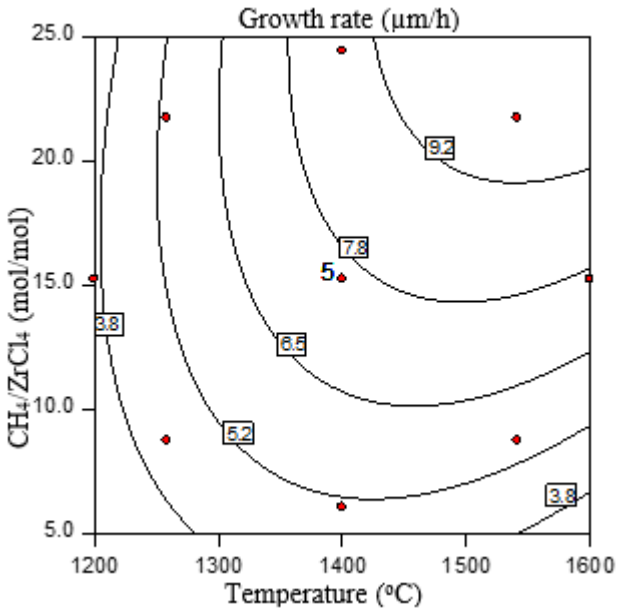

***Figure 7**: The effect of substrate temperature and $CH_4/ZrCl_4$ ratio on growth rate of ZrC. The dots and numerical values are explained in the text.*

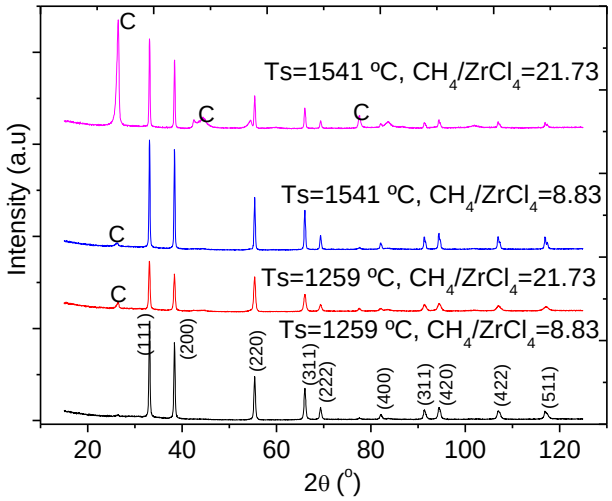

***Figure 8**: Typical XRD pattern for ZrC deposited at 1259 °C and 1541 °C for $CH_4/ZrCl_4$ molar ratio of 8.73 and 21.73.*

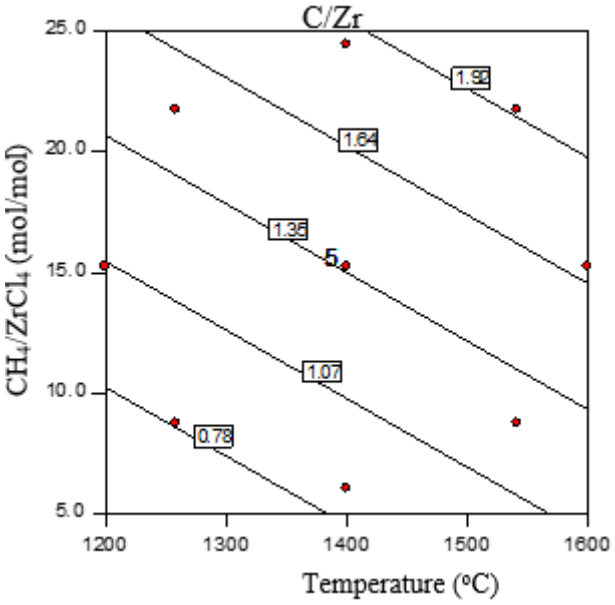

***Figure 9**: The effect of temperature and $CH_4/ZrCl_4$ ratio on C/Zr ratio.*

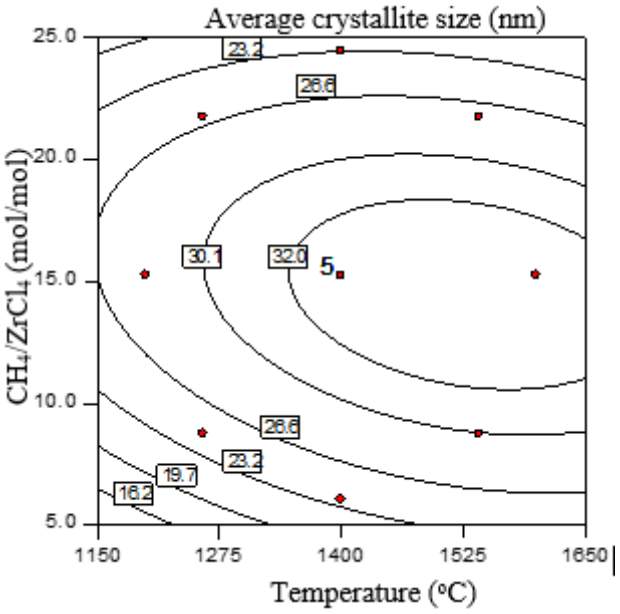

***Figure 10:** The effect of temperature and $CH_4/ZrCl_4$ ratio on crystallite size.*

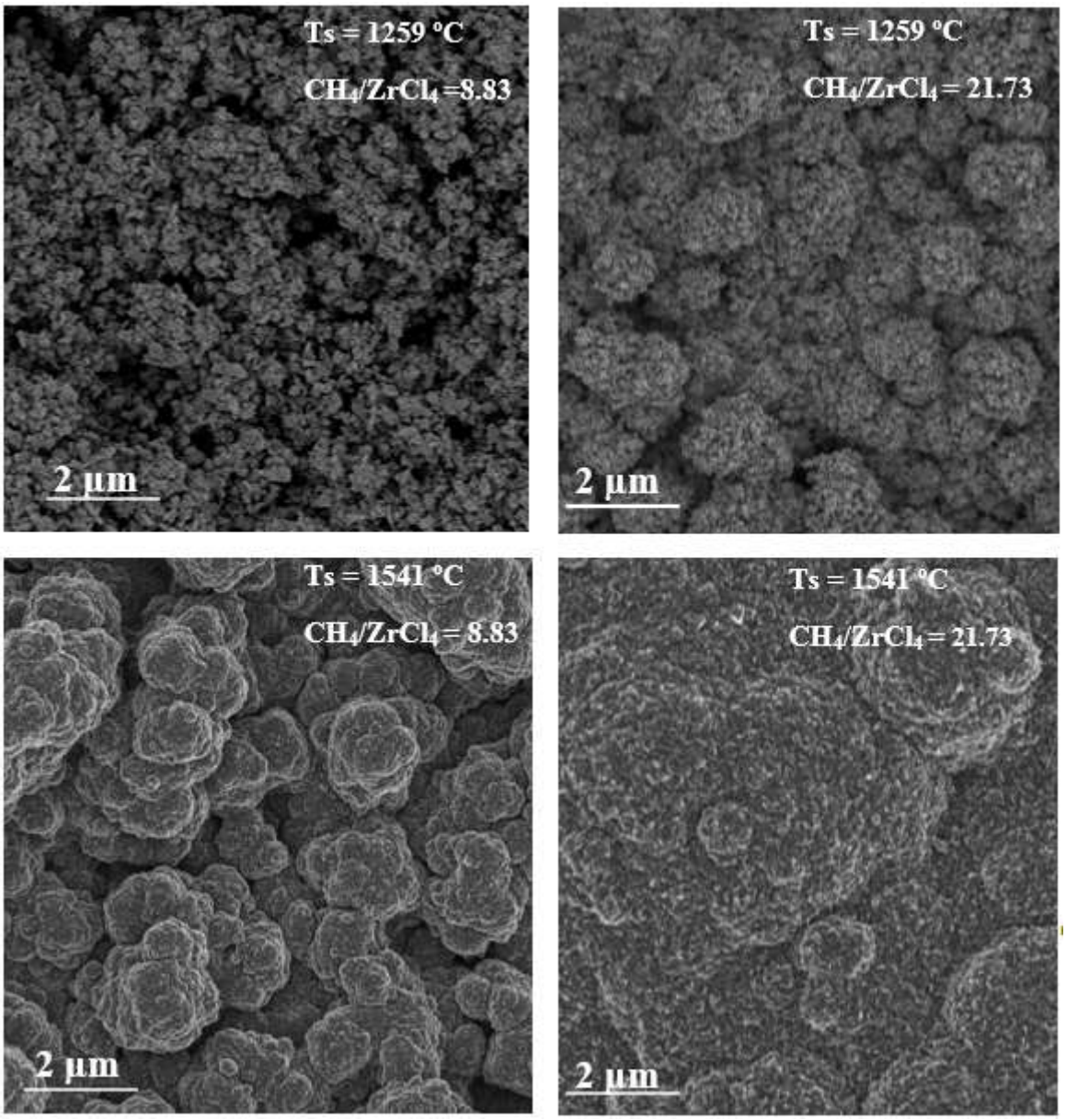

***Figure 11**: FE-SEM image of the surface morphology of ZrC coatings deposited at 1259 ºC and 1541 ºC for $CH_4/ZrCl_4$ molar ratio of 8.73 and 21.73.*

Table

Exp. Number	Point type	Temperature (^oC)	$CH_4/ZrCl_4$	CH_4 flow rate (sccm)	H_2 flow rate (sccm)	Ar flow rate (sccs)	$ZrCl_4$ flow (gh^{-1})
1	Axial	1400	24.44	43.3	853	562	1.0
2	Axial	1400	6.04	10.7	853	562	1.0
3	Factorial	1541	8.73	15.5	853	562	1.0
4	Factorial	1259	21.75	38.5	853	562	1.0
5	Centre	1400	15.24	27.0	853	562	1.0
6	Axial	1600	15.24	27.0	853	562	1.0
7	Centre	1400	15.24	27.0	853	562	1.0
8	Centre	1400	15.24	27.0	853	562	1.0
9	Centre	1400	15.24	27.0	853	562	1.0
10	Factorial	1259	8.73	15.5	853	562	1.0
11	Factorial	1541	21.75	38.5	853	562	1.0
12	Centre	1400	15.24	27.0	853	562	1.0
13	Axial	1200	15.24	27.0	853	562	1.0

Table 1: Parameters for CVD experiments

Exp. Number	Temperature (^oC)	$CH_4/ZrCl_4$	Growth rate (µm/h)	Crystallite size (nm)	C/Zr
1	1400	24.44	9.0	21.8	2.57
2	1400	6.04	5.4	23.9	1.05
3	1541	8.73	5.0	29.1	1.06
4	1259	21.75	5.3	28.4	1.09
5	1400	15.24	7.6	31.9	1.53
6	1600	15.24	8.3	34.1	1.88
7	1400	15.24	7.9	32.0	1.23
8	1400	15.24	7.4	34.2	1.15
9	1400	15.24	7.2	33.4	1.13
10	1259	8.73	4.2	25.8	1.03
11	1541	21.75	9.3	27.8	1.68
12	1400	15.24	7.9	32.6	1.26
13	1200	15.24	3.7	26.3	1.08

Table 2: Experimental results. The growth rate was determined from Equation (3). The average crystallite size was calculated from Scherrer formula given in Equation (6). C/Zr is the ratio of the elemental atomic composition determined by EDS.

Source	Sum of squares	Degrees of freedom	Mean of square	Standard Error	*F*-value	*p*-value Prob > *F*	
Model	39.14	5	7.83	0.12	34.23	< 0.0001	significant
A-Temperature	15.98	1	15.98	0.17	69.88	< 0.0001	
B-$CH_4/ZrCl_4$	13.76	1	13.76	0.17	60.17	0.0001	
AB	2.56	1	2.56	0.24	11.2	0.0123	
A^2	6.44	1	6.44	0.18	28.19	0.0011	
B^2	0.91	1	0.91	0.18	4	0.0857	
Residual	1.6	7	0.23				
Lack of fit	1.22	3	0.41		4.28	0.0969	not significant
Pure error	0.38	4	0.095				
Corrected total	40.74	12					
Standard deviation = 0.48				R^2=0.9607			
Mean = 6.78				Adjusted R^2 =0.9327			
%Coefficient of variation= 7.05				Predicted R^2=0.7724			
Predicted residual error of sums (PRESS)=9.27				Adequate precision=18.85			

Table 3: ANOVA quadratic model results for growth rate (response Y_1**)**

Source	Sum of squares	Degrees of freedom	Mean of square	Standard error	*F*-value	*p*-value Prob > F	
Model	1.38	2	0.69	0.090	6.56	0.0150	Significant
A-Temperature	0.38	1	0.38	0.11	3.65	0.0853	
B-$CH_4/ZrCl_4$	1.0	1	1.00	0.11	9.52	0.0115	
Residual	1.05	10	0.11				
Lack of Fit	0.95	6	0.16		6.15	0.0501	not significant
Pure Error	0.10	4	0.026				
Corrected total	2.44	12					
Standard deviation = 0.32				R^2=0.5683			
Mean = 1.36				Adjusted R^2 = 0.4820			
%Coefficient of variation= 23.76				Predicted R^2= 0.1140			
Predicted residual error of sums (PRESS)= 2.16				Adequate precision= 7.352			

Table 3: ANOVA linear regression model results for C/Zr (response Y_2)

Source	Sum of squares	Degrees of freedom	Mean of square	Standard error	*F*-Value	*p*-value Prob > F	
Model	180.66	5	36.13	0.71	14.14	0.0015	significant
A-Temperature	23.57	1	23.57	0.57	9.22	0.0189	
B-$CH_4/ZrCl_4$	0.35	1	0.35	0.57	0.14	0.7228	
AB	3.8	1	3.8	0.24	1.49	0.262	
A^2	6.92	1	6.92	0.18	2.71	0.1438	
B^2	151.88	1	151.88	0.18	59.44	0.0001	
Residual	17.89	7	2.56				
Lack of fit	14.08	3	4.69		4.93	0.0787	not significant
Pure error	3.81	4	0.95				
Corrected total	198.55	12					
Standard deviation = 1.60					R^2 = 0.9099		
Mean = 29.33					Adjusted R^2 = 0.8456		
%Coefficient of variation = 5.45					Predicted R^2 = 0.4658		
Predicted residual error of sums (PRESS)=106.07					Adequate precision = 9.275		

Table 4: ANOVA quadratic model results for crystallite size (response Y_3)